

Pair plasma relaxation time scales

A.G. Aksenov

*Institute for Computer-Aided Design, Russian Academy of Sciences,
Vtoraya Brestskaya 19/18, 123056 Moscow, Russia*

R. Ruffini and G.V. Vereshchagin

*ICRANet Piazza della Repubblica, 10, 65100 Pescara, Italy and
ICRA and University of Rome "Sapienza", Physics Department, Piazzale A. Moro 5, 00185 Rome, Italy*

Abstract

By numerically solving the relativistic Boltzmann equations, we compute the time scale for relaxation to thermal equilibrium for an optically thick electron-positron plasma with baryon loading. We focus on the time scales of electromagnetic interactions. The collisional integrals are obtained directly from the corresponding QED matrix elements. Thermalization time scales are computed for a wide range of values of both the total energy density (over 10 orders of magnitude) and of the baryonic loading parameter (over 6 orders of magnitude). This also allows us to study such interesting limiting cases as the almost purely electron-positron plasma or electron-proton plasma as well as intermediate cases. These results appear to be important both for laboratory experiments aimed at generating optically thick pair plasmas as well as for astrophysical models in which electron-positron pair plasmas play a relevant role.

PACS numbers: 52.27.Ep, 52.27.Ny, 31.70.Hq

Keywords: pair plasmas, relaxation

Current interest in electron-positron plasmas is due to the exciting possibility of generating such plasmas in laboratory facilities already operating or under construction, see e.g., [1, 2], for a review see [3]. Impressive progress made with ultra-intense lasers [4] has led to the creation of positrons at an unprecedented density of 10^{16} cm^{-3} using ultra-intense short laser pulses, in a region of space with dimensions on the order of the Debye length. However, such densities have not yet reached those necessary for the creation of an optically thick pair plasma [5, 6]. Particle pairs are created at the focal point of ultra-intense lasers via the Bethe-Heitler conversion of hard x-ray bremsstrahlung photons [1] in the collisionless regime [7]. The approach to an optically thick phase may well be envisaged in the near future.

Electron-positron plasmas are known to be present in compact astrophysical objects, leaving their characteristic imprint in the observed radiation spectra [8]. Optically thick electron-positron plasmas do indeed play a crucial role in the gamma-ray burst phenomenon [3, 9].

From the theoretical point of view electron-positron pair plasmas are interesting because of the mass symmetry between the plasma components. This symmetry results in the absence of both acoustic modes and Faraday rotation; waves and instabilities in such plasmas differ significantly from asymmetric electron-ion plasmas, see e.g. [10]. Besides, theoretical progress in understanding quark-gluon plasma in the high-temperature limit is linked to understanding QED plasma since the results in these two cases differ only by trivial factors containing the QCD degrees of freedom (color and flavor) [2].

Most theoretical considerations so far have assumed that an electron-positron plasma is formed either in thermal equilibrium (common temperature, zero chemical po-

tentials) or in chemical equilibrium (nonzero chemical potentials), see e.g. [2] and references therein. However, it is necessary to establish the time scale for actually reaching such a configuration. The only way for particles to thermalize, i.e., reach equilibrium distributions (Bose-Einstein or Fermi-Dirac) is via collisions. Collisions become relevant when the mean free path of the particles becomes smaller than the spatial dimensions of the plasma, and so the optical thickness condition is crucial for thermalization to occur.

Thermalization (chemical equilibration) time scales for optically thick plasmas are estimated in the literature by order of magnitude arguments using essentially just the reaction rates of the dominant particle interaction processes, see e.g. [11, 12]. They have been computed using various approximations. In particular, electrons have been considered ultrarelativistic, and Coulomb logarithm has been replaced by a constant. The accurate determination of such time scales as presented here is instead accomplished by solving the relativistic Boltzmann equations including the collisional integrals representing all possible particle interactions. In this case the Boltzmann equations become highly nonlinear coupled partial integro-differential equations which can only be solved numerically.

We developed a relativistic kinetic code treating the plasma as homogeneous and isotropic and have previously determined the thermalization time scales for an electron-positron plasma for selected initial conditions [13]. This approach was generalized to include protons in [14]. We focus only on the electromagnetic interactions, which have a time scale of less than 10^{-9} sec for our system, and therefore on the proton and leptonic component of the plasma. The presence of neutrons and their possi-

ble equilibrium due to weak interactions will occur only on much longer time scales.

In this paper we report on the systematic results obtained by exploring the large parameter space characterizing pair plasmas with baryonic loading. The two basic parameters are the total energy density ρ and the baryonic loading parameter

$$B \equiv \frac{\rho_b}{\rho_{e,\gamma}} \simeq \frac{n_p m_p c^2}{\rho_{e,\gamma}}, \quad (1)$$

where ρ_b and $\rho_{e,\gamma}$ are respectively the total energy densities of baryons and electron-positron-photon plasma, n_p and m_p are the proton number density and proton mass, and c is the speed of light. We choose the following range of plasma parameters

$$10^{23} \leq \rho \leq 10^{33} \text{ erg/cm}^3, \quad (2)$$

$$10^{-3} \leq B \leq 10^3, \quad (3)$$

allowing us to also treat the limiting cases of almost pure electron-positron plasma with $B \ll 1$, and almost pure electron-ion plasma with $B \simeq m_p/m_e$, respectively. The temperatures in thermal equilibrium corresponding to (2) are $0.1 \lesssim k_B T \lesssim 10 \text{ MeV}$.

Given the smallness of the plasma parameter $g = (n_e \lambda_D^3)^{-1} \ll 1$, where λ_D is the Debye length and n_e is the electron number density, it is sufficient to use one-particle distribution functions. In fact, for the pure electron-positron plasma, the inequality $3 \cdot 10^{-3} \leq g \leq 10^{-2}$ holds in the region of the temperatures of interest. In a homogeneous and isotropic plasma the distribution functions $f(\epsilon, t)$ depend on the energy ϵ of the particle and on the time t . We treat the plasma as nondegenerate, neglecting neutrino channels as well as the creation and annihilation of baryons and the weak interactions [14].

The relativistic Boltzmann equations [15, 16] for photons, electrons, positrons, and protons in our case are

$$\frac{1}{c} \frac{\partial f_i}{\partial t} = \sum_q (\eta_i^q - \chi_i^q f_i), \quad (4)$$

where the index i denotes the type of particle and η_i^q, χ_i^q are the emission and the absorption coefficients for the production of the i th-particle via the reaction labeled by q . We account for all relevant binary and triple interactions between electrons, positrons, photons, and protons as summarized in Tables I and II.

It has been shown [13] that independent of the functional form of the initial distribution functions $f_i(\epsilon, 0)$, plasma evolves to a thermal equilibrium state through the kinetic equilibrium, when the distribution functions of all the particles acquire the same form

$$f_i(\epsilon) = \exp\left(-\frac{\epsilon - \varphi_i}{\theta_i}\right), \quad (5)$$

| Binary interactions | Radiative and pair producing variants |
|---|---|
| Møller and Bhabha $e_1^\pm e_2^\pm \rightarrow e_1^{\pm'} e_2^{\pm'}$ $e^\pm e^\mp \rightarrow e^{\pm'} e^{\mp'}$ | Bremsstrahlung $e_1^\pm e_2^\pm \leftrightarrow e_1^{\pm'} e_2^{\pm'} \gamma$ $e^\pm e^\mp \leftrightarrow e^{\pm'} e^{\mp'} \gamma$ |
| Single Compton $e^\pm \gamma \rightarrow e^\pm \gamma'$ | Double Compton $e^\pm \gamma \leftrightarrow e^{\pm'} \gamma' \gamma''$ |
| Pair production and annihilation $\gamma \gamma' \leftrightarrow e^\pm e^\mp$ | Radiative pair production and 3-photon annihilation $\gamma \gamma' \leftrightarrow e^\pm e^\mp \gamma''$ $e^\pm e^\mp \leftrightarrow \gamma \gamma' \gamma''$ |
| | $e^\pm \gamma \leftrightarrow e^{\pm'} e^{\mp'} e^{\pm''}$ |

TABLE I: Microphysical processes in the pair plasma.

| Binary interactions (Coulomb scattering) | Radiative and pair producing variants |
|---|--|
| $p_1 p_2 \rightarrow p_1' p_2'$ | $p e^\pm \leftrightarrow p' e^{\pm'} \gamma$ |
| $p e^\pm \rightarrow p' e^{\pm'}$ | $p \gamma \leftrightarrow p' e^\pm e^\mp$ |

TABLE II: Microphysical processes in the pair plasma involving protons. For details see also [3].

where $\epsilon_i = \epsilon_i/(m_i c^2)$ is the energy of the particles, $\varphi_i \equiv \mu_i/(m_i c^2)$ and $\theta_i \equiv k_B T_i/(m_i c^2)$ are their chemical potentials and temperatures, and k_B is Boltzmann's constant. The unique signature of kinetic equilibrium is the equal temperatures of all the particles and the nonzero chemical potential of the photons. In fact the same is also true for a pair plasma with proton loading [14]. The approach to complete thermal equilibrium is more complicated in this latter case and depends on the baryon loading. For $B \ll \sqrt{m_p/m_e}$, protons are rare and thermalize via proton-electron (positron) elastic scattering, while in the opposite case $B \gg \sqrt{m_p/m_e}$, proton-proton Coulomb scattering dominates over the proton-electron scattering and brings protons into thermal equilibrium first with themselves. Then protons thermalize with the pair plasma through triple interactions, for details see [14]. The two-body time scales involving protons should be compared with the three-body time scales bringing the electron-positron-photon plasma into thermal equilibrium. In fact we found that for $B \ll 1$, the electron-positron-photon plasma reaches thermal equilibrium at a given temperature, while protons reach thermal equilibrium with themselves at a different temperature; only later the plasma evolves to complete thermal equilibrium with the single temperature on a time scale

$$\tau_{th} \simeq \text{Max}[\tau_{3p}, \text{Min}(\tau_{ep}, \tau_{pp})], \quad (6)$$

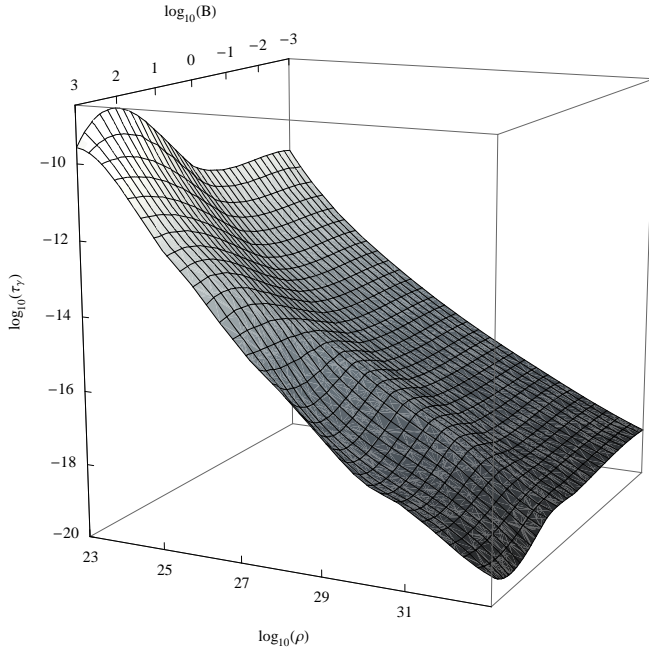


FIG. 1: The thermalization time scale of the electron-positron-photon component of plasma as a function of the total energy density and the baryonic loading parameter. The energy density is measured in erg/cm^3 , time is seconds.

where

$$\tau_{ep} \simeq \frac{m_p c}{\epsilon_e \sigma_T n_e}, \quad (7)$$

$$\tau_{pp} \simeq \sqrt{\frac{m_p}{m_e}} (\sigma_T n_p c)^{-1}, \quad (8)$$

$$\tau_{3p} \simeq (\alpha \sigma_T n_e c)^{-1} \quad (9)$$

are the proton-electron (positron) elastic scattering time scale, the proton-proton elastic scattering time scale, and the three-particle interaction time scale respectively, while σ_T is the Thomson cross-section and α is the fine structure constant. In (7)–(9) the energy dependence of the corresponding time scales is neglected.

The chemical relaxation (thermalization) time scale is usually computed as

$$\tau_i = \lim_{t \rightarrow \infty} \left\{ [F_i(t) - F_i(\infty)] \left(\frac{dF_i}{dt} \right)^{-1} \right\}, \quad (10)$$

where $F_i = \exp(\varphi_i/\theta_i)$ is the fugacity of a particle of type i . Instead of F_i we use one of the quantities θ_i , φ_i , n_i , or ρ_i in this computation.

We solved the Boltzmann equations with parameters (ρ, B) in the range given by Eqs. (2) and (3). In total 78 models were computed, starting from a nonequilibrium configuration until reaching a steady state solution on the computational grid with 20 intervals for the particle energy and 16 intervals for the angles, for details

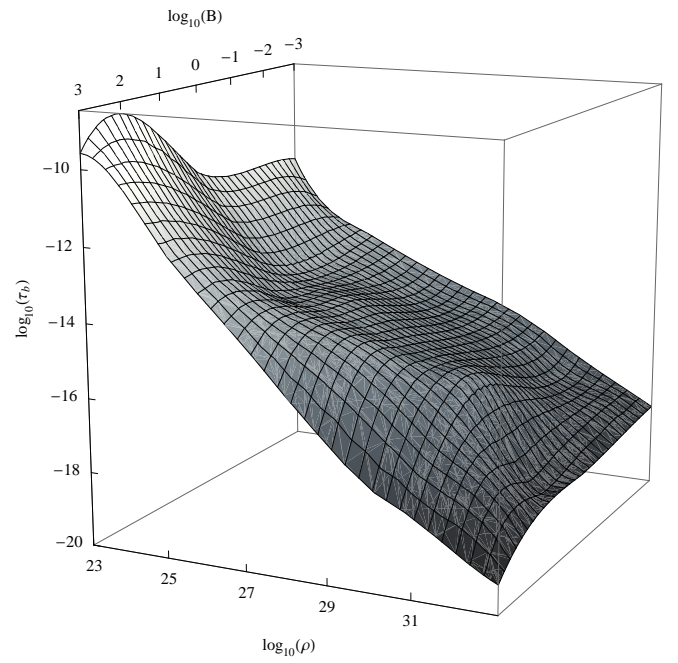


FIG. 2: The final thermalization time scale of a pair plasma with baryonic loading as a function of the total energy density and the baryonic loading parameter. The energy density is measured in erg/cm^3 , time is seconds.

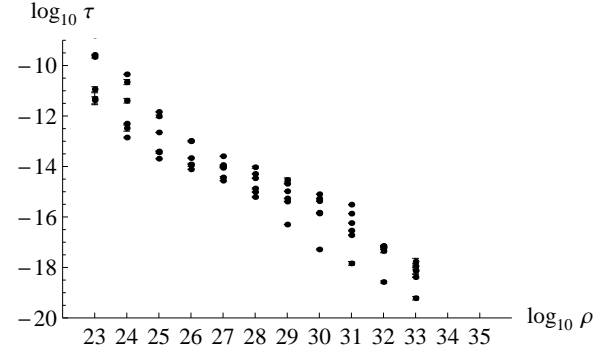


FIG. 3: The final thermalization time scale of pair plasma with baryonic loading as a function of the total energy density for selected values of the baryonic loading parameter $B = (10^{-3}, 10^{-1.5}, 1, 10, 10^2, 10^3)$. The energy density is measured in erg/cm^3 , time is seconds. Error bars correspond to one standard deviation of the time scale (11) away from the average value τ_{th} over the interval $t_{in} \leq t \leq t_{fin}$.

see [14]. For each model we computed the corresponding time scales for all particles of the i th kind. For practical purposes, instead of (10) we used the following approximation

$$\tau_{th} = \frac{1}{t_{fin} - t_{in}} \int_{t_{in}}^{t_{fin}} [\theta(t) - \theta(t_{\max})] \left(\frac{d\theta}{dt} \right)^{-1} dt, \quad (11)$$

with $t_{in} < t_{fin} < t_{\max}$, where t_{\max} is the moment of time where the steady solution is reached and t_{in} and t_{fin} are

the boundaries of the time interval over which the averaging is performed, for details see [17]. The thermalization

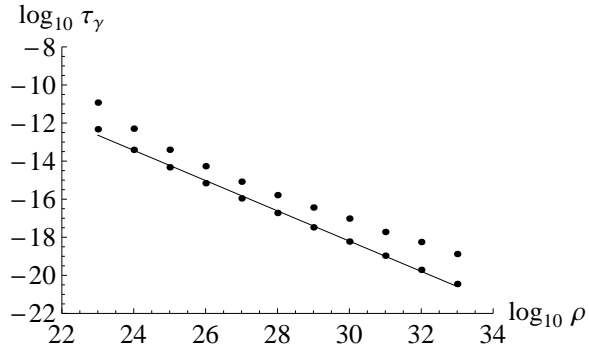


FIG. 4: The thermalization time scale of the electron-positron-photon component of the plasma as a function of the total energy density (points), compared with the τ_{3p} time scale (joined points) computed using (9) for $B = 1$. The energy density is measured in erg/cm^3 , time is seconds.

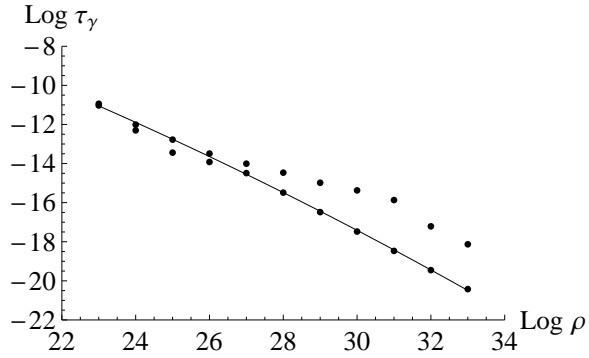


FIG. 5: The final thermalization time scale of a pair plasma with baryonic loading as a function of the total energy density (points), compared with the τ_{th} time scale (joined points) computed using (6) for $B = 1$. The energy density is measured in erg/cm^3 , time is seconds.

time scale of the electron-positron-photon component is shown in Fig. 1 as a function of the total energy density of the plasma and the baryonic loading parameter. The time scales of electrons, positrons and photons coincide. The final thermalization time scale of pair plasma with baryonic loading is shown in Fig. 2. Its dependence on either variable cannot be fit by a simple power law, although it decreases monotonically with increasing total energy density, while it is not even a monotonic function of the baryonic loading parameter.

In Fig. 3 the final thermalization time scale is shown for all the models we computed, along with the “error bars” which mark one standard deviation of the time scale (11) away from the average value τ_{th} in the averaging interval $t_{in} \leq t \leq t_{fin}$. The largest source of error comes from the small values of the time derivative in (11), although errors are typically below a few percent.

In Fig. 4 we compare for $B = 1$ the actual value of the thermalization time scale of the electron-positron-photon component with the value estimated from (9). Both values clearly differ significantly. Actually the systematic underestimation by more than one order of magnitude which occurs for $B \leq 1$ disappears for larger baryonic loading.

In Fig. 5 we present the computed values of the final thermalization time scale of the pair plasma with baryonic loading together with the value estimated from (6), again for $B = 1$. Unlike the previous case, the final thermalization time scale is a more complex function of the total energy density. Interestingly, less significant deviations from the value (6) occur at the extremes of the interval (3).

In this paper we have computed for the first time the time scale of thermalization for an electron-positron plasma with proton loading over wide ranges of both the total energy density (10 orders of magnitude) and baryonic loading parameter (6 orders of magnitude) allowing the treatment of the limiting cases of almost pure electron-positron plasma, almost pure electron-ion plasma as well as intermediate cases. The final result is presented in Fig. 1 and 2. The relaxation to thermal equilibrium for the total energy density (2) always occurs on a time scale less than 10^{-9} sec. It is interesting that the electron-positron-photon component and/or proton component can thermalize earlier than the time at which complete thermal equilibrium is reached. The relevant time scales are given and compared with the order-of-magnitude estimates. Unlike previous work there are no simplifying assumptions in our method since collisional integrals in the Boltzmann equations are computed directly from the corresponding QED matrix elements, e.g. from the first principles.

These results may be of relevance for the ongoing and future laboratory experiments aimed at creating electron-positron plasmas. Current optical lasers producing pulses during $\sim 10^{-15}$ sec carrying energy $\sim 10^2$ J = 10^9 erg are capable to produce positrons with the number density 10^{16} cm^{-3} [4]. There are claims that densities of the order of 10^{22} cm^{-3} are reachable [18]. These densities today are yet far from 10^{28} cm^{-3} required for the plasma with the size $r_0 \simeq \mu\text{m}$ to be optically thick [5]. Notice, that the expansion timescale of such plasma will be $r_0/c \sim 10^{-14}$ sec, while the timescale to establish kinetic equilibrium for the number density considered is of the same order of magnitude. These arguments show that theoretical results obtained assuming thermal or kinetic equilibrium, such as in [2], cannot be applied to pair plasma, generated by ultraintense lasers.

However, results presented in this paper are important for understanding astrophysical systems observed today in which optically thick electron-positron plasmas are present. As specific example we recall that electron-positron pairs play the crucial rule in the dynamics of

GRB sources. Considering typical energies and initial radii for GRB progenitors [19]

$$10^{48}\text{erg} < E_0 < 10^{54}\text{erg}, \quad 10^7\text{cm} < R_0 < 10^8\text{cm}, \quad (12)$$

we estimate the range for the energy density in GRB sources

$$10^{23}\frac{\text{erg}}{\text{cm}^3} < \rho < 10^{32}\frac{\text{erg}}{\text{cm}^3}, \quad (13)$$

which coincides with (2). As for the baryonic loading of GRBs it is typically in the lower range of (2), namely [9]

$$10^{-3} < B < 10^{-2}. \quad (14)$$

Such high energy density leads to large number density of electron-positron pairs in the source of GRB, of the order of

$$10^{30}\text{cm}^{-3} < n < 10^{37}\text{cm}^{-3}, \quad (15)$$

making it opaque to photons with huge optical depth of the order of

$$10^{13} < \tau < 10^{18}. \quad (16)$$

In fact, the radiative pressure of optically thick electron-positron plasma in these systems is responsible for the effect of accelerated expansion [9, 20–22], leading to unprecedented Lorentz factors attained $\Gamma \simeq B^{-1}$, up to 10^3 , see e.g. [23, 24]. The role of the baryon admixture in electron-positron plasma in GRBs is to transfer internal energy of pairs and photons into kinetic energy of the bulk motion thus giving origin to afterglows of GRBs [9, 19]. Notice that in GRBs the timescales of thermalization are much shorter than the dynamical timescales $R_0/c \sim 10^{-3}$ sec, which implies that expanding electron-positron plasma even in the presence of baryons is in thermal equilibrium during the accelerating optically thick phase [25].

After completion of this work we learned about the publication of [26] where work similar to ours has been performed. Between this paper and our work conceptual differences should be noted which concern the attribution of thermalization to two-body Møller and Bhabha scattering, while we have pointed out explicitly that three-body interactions play an essential role. The thermalization time scales obtained by us have been computed with reference to these three-body interactions.

Acknowledgements. We thank both anonymous referees for their comments which allowed to improve remarkably the paper.

-
- [1] J. Myatt et al., Phys. Rev. E **79**, 066409 (2009).
 - [2] M. H. Thoma, Reviews of Modern Physics **81**, 959 (2009).
 - [3] R. Ruffini, G. Vereshchagin, and S.-S. Xue, Phys. Rep. **487**, 1 (2010).
 - [4] H. Chen et al., Phys. Rev. Lett. **102**, 105001 (2009).
 - [5] J. I. Katz, ApJS **127**, 371 (2000).
 - [6] M. G. Mustafa and B. Kämpfer, Phys. Rev. A **79**, 020103 (2009).
 - [7] S. C. Wilks, W. L. Kruer, M. Tabak, and A. B. Langdon, Physical Review Letters **69**, 1383 (1992).
 - [8] E. Churazov, R. Sunyaev, S. Sazonov, M. Revnivtsev, and D. Varshalovich, MNRAS **357**, 1377 (2005).
 - [9] R. Ruffini et al., The Blackhole energy and the canonical Gamma-Ray Burst IV: the “long,” “genuine short” and “fake-disguised short” GRBs, in *American Institute of Physics Conference Series*, edited by M. Novello and S. Perez, volume 1132 of *American Institute of Physics Conference Series*, pages 199–266, 2009.
 - [10] G. P. Zank and R. G. Greaves, Phys. Rev. E **51**, 6079 (1995).
 - [11] R. J. Gould, Physics of Fluids **24**, 102 (1981).
 - [12] S. Stepney, MNRAS **202**, 467 (1983).
 - [13] A. G. Aksenov, R. Ruffini, and G. V. Vereshchagin, Phys. Rev. Lett. **99**, 125003 (2007).
 - [14] A. G. Aksenov, R. Ruffini, and G. V. Vereshchagin, Phys. Rev. D **79**, 043008 (2009).
 - [15] S. Belyaev and G. Budker, DAN SSSR **107**, 807 (1956).
 - [16] D. Mihalas and B. W. Mihalas, *Foundations of Radiation Hydrodynamics*, New York, Oxford University Press, 1984.
 - [17] A. G. Aksenov, R. Ruffini, and G. V. Vereshchagin, AIP Conf. Proc. **1205**, 11 (2010).
 - [18] B. Shen and J. Meyer-Ter-Vehn, Phys. Rev. E **65**, 016405 (2002).
 - [19] T. Piran, Phys. Rep. **314**, 575 (1999).
 - [20] R. Ruffini, J. D. Salmonson, J. R. Wilson, and S.-S. Xue, A&A **350**, 334 (1999).
 - [21] R. Ruffini, J. D. Salmonson, J. R. Wilson, and S.-S. Xue, A&A **359**, 855 (2000).
 - [22] C. L. Bianco, R. Ruffini, G. Vereshchagin, and S.-S. Xue, J.Korean Phys.Soc. **49**, 722 (2006).
 - [23] A. A. Abdo et al., Science **323**, 1688 (2009).
 - [24] L. Izzo et al., in *Proceedings of the First Galileo - Xu Guangqi meeting held in October 26-30, 2009 Shanghai (China)*, in press, 2010.
 - [25] A. G. Aksenov, C. L. Bianco, R. Ruffini, and G. V. Vereshchagin, AIP Conf. Proc. **1000**, 309 (2008).
 - [26] I. Kuznetsova, D. Habs, and J. Rafelski, ArXiv e-print arXiv0911.0118 (2009).